Vulnerability assessment of buildings based on the pseudo-dynamic testing method with sub-structuring: application to progressive collapse

Jean-Baptiste Charrié, D. Bertrand, Cédric Desprez, Stéphane Grange

COMPDYN 2023
9th ECCOMAS Thematic Conference on
Computational Methods in Structural Dynamics and Earthquake Engineering
M. Papadrakakis, M. Fragiadakis (eds.)
Athens, Greece, 12-–14 June 2023

VULNERABILITY ASSESSMENT OF BUILDINGS BASED ON THE PSEUDO-DYNAMIC TESTING METHOD WITH SUB-STRUCTURING: APPLICATION TO PROGRESSIVE COLLAPSE

Jean-Baptiste Charrié[1], David Bertrand[1], Cédric Desprez[1], Stéphane Grange[1]

[1]Univ Lyon, INSA Lyon, GEOMAS, EA7495
69621 Villeurbanne, France
e-mail: {jean-baptiste.charrie, david.bertrand, cedric.desprez, stephane.grange}@insa-lyon.fr

Keywords: Progressive collapse, Pseudo-dynamic testing, Sub-structuring, Reinforced concrete modeling, Dynamic behavior

Abstract. *Due to various natural or anthropogenic hazards, buildings' structural members can lose their bearing capacities which can lead to the building's progressive collapse. The latter subject is of growing interest regarding the socio-economic context [1]. Academic research on progressive collapse took off in the early 2000s, with the 9/11 attacks on the Twin Towers (NY, 2001) [1]. Analyses on large structures are mainly done numerically. On the other side, most experiments are lead on smaller structural elements. Until now, these experiments have been limited by dimensions, dynamic forces and real-time control capabilities. In earthquake engineering, the pseudo-dynamic method (PsD) is often used [2]. Experimental tests are performed quasi-statically on a structural part, while the inertial forces are computed within a time integration scheme. An extension of the method is the sub-structured PsD trials, which consists of inserting the tested part in a larger finite element mesh. Sub-structuring enables accounting for the whole structure's effect on the tested part [3]. The paper presents a first experimental campaign, which validated the interest of the approach on a simple structural part. Another experimental campaign is underway, on larger structural members to further comfort the method's validity to study progressive collapse.*

1 INTRODUCTION

The paper aims at studying the sudden loss of bearing capacity in civil engineering structures. Loss of bearing capacity has been of growing interest for the past two decades, especially after the terrorist attacks on the World Trade Center (NY, 2001)[1]. The phenomenon leads to partial or complete structural collapse. Origins are diverse, from gas explosions to natural or anthropogenic risks, including design defects, building decay, *etc*.

New knowledge is still needed to propose new structures capable of mitigating damages due to such events, whilst maintaining structural and/or functional integrity, as well as retro-fitting real-estate to prolong existing buildings' lives. Approaches to characterize structural integrity remains largely experiment based, to validate numerical models. To guarantee representative results, full scale experiments are needed. This point is often a limiting factor due to the scale of civil engineering structures; logistics, costs and dynamic solicitation of large masses are all drawbacks to this approach. This is all the more true for larger structures, and when the damaged zone is limited.

For those reasons, a novel approach is proposed to tackle those problems, taking advantage of the Pseudo-Dynamic (PsD) method. The latter is largely used in earthquake engineering, to test dynamic responses of building in a *quasi*-static manner [2]. Combined with a sub-structuring approach, the resulting tests will resolve scale, resulting forces and logistical problems to some extent [3]. Sub-structured PsD testing has never been used in progressive collapse experiments. This paper presents this promising alternative to currently used methods. As well as greatly reducing costs, experimental implementation is simplified. From an experimental point of view, the structure's static response is needed, whereas the dynamic behavior is accounted for numerically. Thus, testing is simpler, with smaller forces, lower data acquisition, and time dilation. Better control during trials yield more repeatability, and should enable parametric studies with a high confidence degree in the results.

Foremost, the PsD testing approach with sub-structuring is presented. Then, the two experimental campaigns, representing accidental loss of bearing scenarios are proposed. The first campaign is a proof-of-concept to demonstrate the method's legitimacy to investigate progressive collapse events. The second experimental campaign's aim is to further validate the method, with larger, more intricate structural members, and better boundary conditions (BCs). Additional phenomenons will be highlighted, such as Tensile Catenary Action (TCA) and Compressive Arch Action (CAA) [1]. The first campaign's results are compared and validated using a non-linear, Finite Element (FE), multi-fiber model. Finally, results are discussed, and the second experimental campaigns objectives and perspectives are presented.

2 METHODOLOGY

2.1 Pseudo-Dynamic testing algorithm

2.1.1 Classic Pseudo-Dynamic method

The algorithm used is an α Operator-Splitting (α-OS). It is particularly suited as it is implicit and non-iterative [2]. Eq. (1) gives the relationship at time $t_{n+1} = t_n + \Delta t$, with n being the time increment index.

$$\mathbb{M}\boldsymbol{a}^{n+1} + \mathbb{C}\boldsymbol{v}^{n+1} + \boldsymbol{R}(\boldsymbol{d}^{n+1}) = \boldsymbol{F}_{ext}^{n+1} \tag{1}$$

$\mathbb{M}$ and $\mathbb{C}$ are respectively the mass and damping matrices. $\boldsymbol{d}$, $\boldsymbol{v}$ and $\boldsymbol{a}$ are the nodal displacements, velocities and accelerations. $\boldsymbol{F}_{ext}$ are the external forces and $\boldsymbol{R}$ the restoring forces,

measured statically on the tested structure.

The α-OS scheme is based on a predictor-corrector procedure. The prediction step is given by Eq. (2) :

$$\text{Prediction} \begin{cases} \tilde{\boldsymbol{d}}^{n+1} & = \boldsymbol{d}^n + \Delta t\, \boldsymbol{v}^n + \frac{\Delta t^2}{2}(1-2\beta)\boldsymbol{a}^n \\ \tilde{\boldsymbol{v}}^{n+1} & = \boldsymbol{v}^n + \Delta t\,(1-\gamma)\boldsymbol{a}^n \end{cases} \tag{2}$$

The coefficients β and γ depend on α, the scheme's parameter: $\beta = \frac{(1-\alpha)^2}{4}$ and $\gamma = \frac{1-2\alpha}{2}$. Once the desired predicted displacements $\tilde{\boldsymbol{d}}^{n+1}$ have been imposed, the experimental system fetches the measured displacements and forces: $\tilde{\boldsymbol{d}}_m^{n+1}$ and $\tilde{\boldsymbol{R}}_m^{n+1}$. The acceleration vector is then computed (Eq. (3) using the pseudo-mass matrix $\hat{\mathbb{M}}$ (Eq. (4)) and the α-shifted pseudo-force vector $\hat{\boldsymbol{f}}^{n+1+\alpha}$ (Eq. (5)).

$$\boldsymbol{a}^{n+1} = \hat{\mathbb{M}}^{-1}\,\hat{\boldsymbol{f}}^{n+1+\alpha} \tag{3}$$

$$\hat{\mathbb{M}} = \mathbb{M} + \gamma\,\Delta t\,(1+\alpha)\mathbb{C} + \beta\,\Delta t^2\,(1+\alpha)\mathbb{K}^{\mathbb{I}} \tag{4}$$

$$\begin{aligned} \hat{\boldsymbol{f}}^{n+1+\alpha} = {} & (1+\alpha)\,\boldsymbol{F}_{ext}^{n+1} - \alpha\,\boldsymbol{F}_{ext}^{n} + \alpha\,\tilde{\boldsymbol{R}}^n - (1+\alpha)\tilde{\boldsymbol{R}}^{n+1} + \dots \\ & \dots + \alpha\,\mathbb{C}\,\tilde{\boldsymbol{v}}^n - (1+\alpha)\,\mathbb{C}\,\tilde{\boldsymbol{v}}^{n+1} + \alpha(\gamma\,\Delta t\,\mathbb{C} + \beta\,\Delta t^2\,\mathbb{K}^I)\boldsymbol{a}^n \end{aligned} \tag{5}$$

To guarantee the algorithm's convergence, the stiffness matrix $\mathbb{K}^{\mathbb{I}}$ used to compute $\hat{\mathbb{M}}$ must be as close as possible to the initial elastic stiffness matrix, and greater than the current tangent matrix [2]. To compensate for measurement errors without iterating, the restoring forces are estimated from the imposed predicted displacement (eq. (6)).

$$\tilde{\boldsymbol{R}}^{n+1} \approx \tilde{\boldsymbol{R}}_m^{n+1} + \mathbb{K}^I\left[\tilde{\boldsymbol{d}}_m^{n+1} - \tilde{\boldsymbol{d}}^{n+1}\right] \tag{6}$$

Once $\tilde{\boldsymbol{R}}^{n+1}$ is computed, $\hat{\boldsymbol{f}}^{n+1+\alpha}$ can be calculated to get $\boldsymbol{a}^{n+1}$. Finally, the kinematic field is corrected (eq. (7))

$$\text{Correction} \begin{cases} \boldsymbol{d}^{n+1} & = \tilde{\boldsymbol{d}}^{n+1} + \beta\Delta t^2\,\boldsymbol{a}^{n+1} \\ \boldsymbol{v}^{n+1} & = \tilde{\boldsymbol{v}}^{n+1} + \gamma\Delta t\,\boldsymbol{a}^{n+1} \end{cases} \tag{7}$$

2.1.2 Sub-Structuring method

Sub-structuring allows for part of the structure to be simulated (S), while only the critical part is physically tested (T) under *quasi*-static conditions. A domain decomposition is done on the equations presented above to separate the simulated and tested parts. The resolution process is based on [3], and can be written as:

$$\begin{bmatrix} {}^S\hat{M}_{ij} & {}^S\hat{M}_{i\theta} & 0 \\ {}^S\hat{M}_{\delta j} & {}^S\hat{M}_{\delta\theta} + {}^T\hat{M}_{\delta\theta} & {}^T\hat{M}_{\delta J} \\ 0 & {}^T\hat{M}_{I\theta} & {}^T\hat{M}_{IJ} \end{bmatrix} \begin{bmatrix} a_j^{n+1} \\ a_\theta^{n+1} \\ a_J^{n+1} \end{bmatrix} = \begin{bmatrix} {}^S\hat{f}_i^{n+1+\alpha} \\ {}^S\hat{f}_\delta^{n+1+\alpha} + {}^T\hat{f}_\delta^{n+1+\alpha} \\ {}^T\hat{f}_I^{n+1+\alpha} \end{bmatrix} \tag{8}$$

Indices I and J (resp. i and j) refer to tested (resp. simulated) Degrees of Freedom (DOFs). Interface DOFs are index δ and θ. To treat simulated and tested parts in parallel, a static condensation is performed. The pseudo-mass matrix is generated, then accelerations of the modeled part's DOFs are condensed onto the tested part (Eq. (9) using the first line of Eq.(8)).

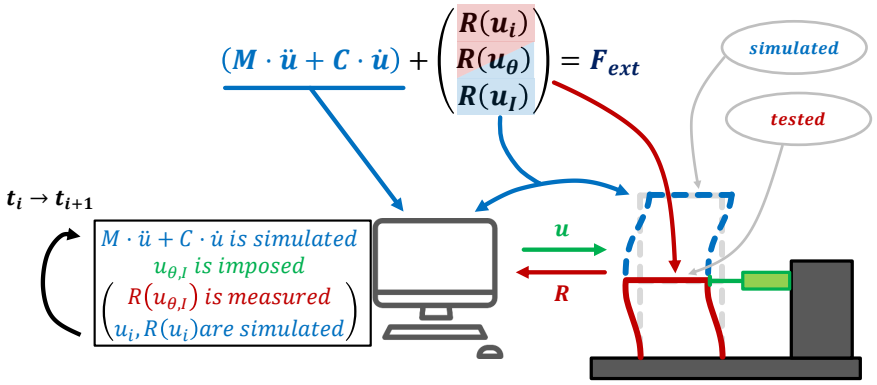

Figure 1: Principle of the sub-structured PsD tests' procedure. Red part is tested, blue part is modeled using FEM. Actuators are represented in green.

$$ {}^{S}\hat{M}_{ij} a_j^{n+1} = {}^{S}\hat{f}_i^{n+1+\alpha} - {}^{S}\hat{M}_{i\theta} a_\theta^{n+1} \tag{9} $$

Then, Eq. (9) is injected onto Eq. (8)'s second and third line:

$$ \begin{bmatrix} {}^{T}\hat{M}_{\delta\theta} + {}^{SC}\hat{M}_{\delta\theta} & {}^{T}\hat{M}_{\delta J} \\ {}^{T}\hat{M}_{I\theta} & {}^{T}\hat{M}_{IJ} \end{bmatrix} \begin{bmatrix} a_\theta^{n+1} \\ a_J^{n+1} \end{bmatrix} = \begin{bmatrix} {}^{T}\hat{f}_\delta^{n+1+\alpha} + {}^{SC}\hat{f}_\delta^{n+1+\alpha} \\ {}^{T}\hat{f}_I^{n+1+\alpha} \end{bmatrix} \tag{10} $$

With ${}^{SC}\hat{M}_{\delta\theta} = {}^{S}\hat{M}_{\delta\theta} - {}^{S}\hat{M}_{\delta j} {}^{S}\hat{M}_{ji}{}^{-1} {}^{S}\hat{M}_{i\theta}$ and ${}^{SC}\hat{f}_\delta^{n+1+\alpha} = {}^{S}\hat{f}_\delta^{n+1+\alpha} - {}^{S}\hat{M}_{\delta j} {}^{S}\hat{M}_{ji}{}^{-1} {}^{S}\hat{f}_i^{n+1+\alpha}$.

2.2 Experimental setups

2.2.1 Campaign 00 - 2021

As a proof of concept for PsD based progressive collapse trials, four Reinforced Concrete (RC) beams were made. For the sake of simplicity, boundary conditions and geometry were as simple as possible. The beams' responses were characterized by two pushovers tests done at different loading rates to validate that the static response is independent of load rate. A first, classic PsD test was conducted, serving as a reference trial. The last beam was tested using a sub-structured PsD test. Results will be discussed in this section.

RC beam characteristics Beams were poured using $C25/30$ concrete, along with $HA500\,B$ steel rebars. Reinforcements were designed according to Eurocode 2 recommendations, for a $20kN$ ultimate load in a three points bending test configuration. Dimensions and details are depicted in Figure (2).

Trials were conducted after 28 days of curing or more. Compression and Brazilian tests on $11 \cdot 22cm$ cylindrical samples yielded the following results: $f_{cm} = 29.75MPa$ and $f_{ctm} = 2.79MPa$.

Experimental setup Each beam is simply supported at each end, with a $2.12m$ span. An hydraulic actuator controls the beam's mid-span displacement. A force sensor is bolted on the actuator's head, in contact with a steel plate located on the beam's upper surface at mid-span. A diffuse light device shines on the freckled center zone of the beam. A camera captures the zone of interest during the test, for Digital Image Correlation (DIC) measurements. The setup is shown in Figure (3).

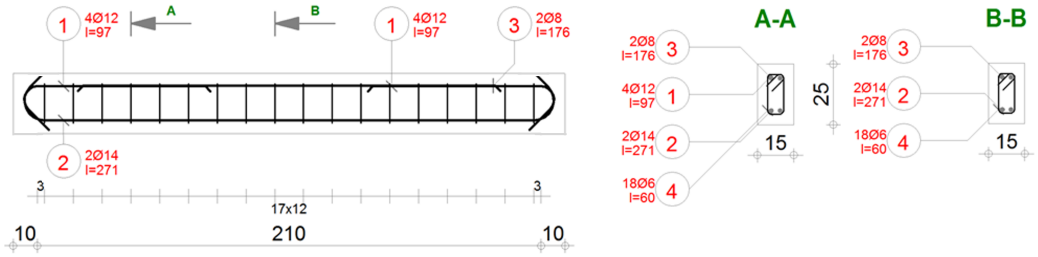

Figure 2: Beam and reinforcement dimensions (cm) - Campaign 00, 2021

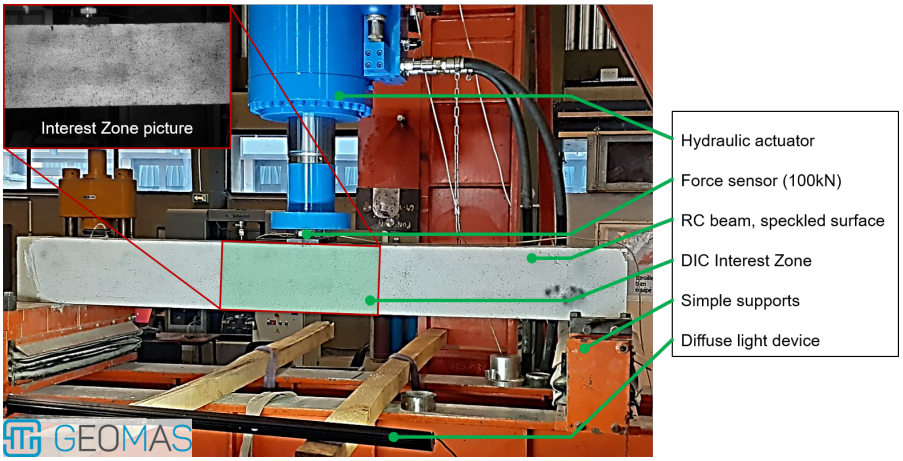

Figure 3: Experimental setup - Campaign 00, 2021

Pushover tests Two beams are subjected to a pushover test in three points bending conditions. To assess load rate dependency, two settings are used: 10mm/s for `Beam1P0` and 0.032 mm/s for `Beam2P0`.

Classic PsD test The classic PsD test is done on beam `Beam4PsDB`. Its response is that of a simply supported beam, carrying $M_p = 4500kg$, a *virtual* load taken into account using the PsD method. At time $t = 0s$, gravity is applied, simulating a bearing loss at mid-span. The system responses as a single DOF, and viscous damping is considered : $c = 2\xi\sqrt{K^I M_p}$; with $\xi = 5\%$, and $K^I = 5.7 \cdot 10^6 N.m^{-1}$ the averaged initial stiffness of beams `Beam1PO` and `Beam2PO`. The experimental setup is described in Figure (3).

Sub-structured PsD test PsD using sub-structuring is done on `Beam3PsDSS`: the experimental beam is part of a larger numerical model. The structure is meshed and modeled using 2D, *Euler-Bernoulli* kinematic Finite Elements, with 3 FEs along each post and beam. Only the lower beam is not modeled, as it corresponds to the experimental sub-structure. The full model is described in Figure (4).

For the sake of simplicity, the simulated part is considered elastic. Furthermore, the response is assumed symmetrical as the bearing loss happens on the central post. The following numerical values are used: a *Young*'s modulus of $21GPa$, a density of $2500kg$, and 5% Rayleigh damping (applied on the 1^{st} and 5^{th} eigenmodes). Using those values, the numerical beams have stiffness values equivalent to those of the experimental ones.

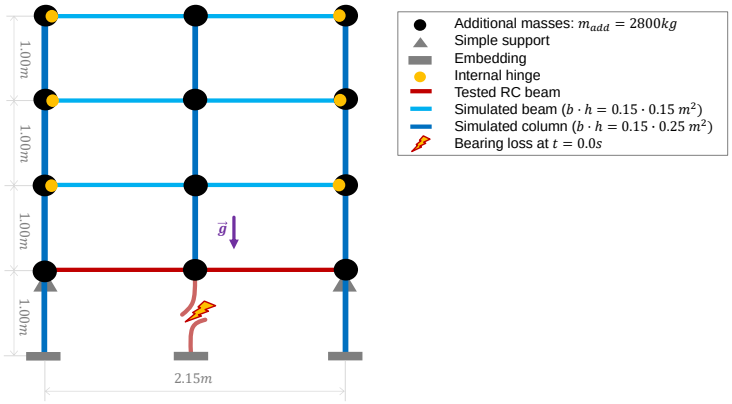

Figure 4: Diagram for the simple PsD test (`Beam4PsDB`)

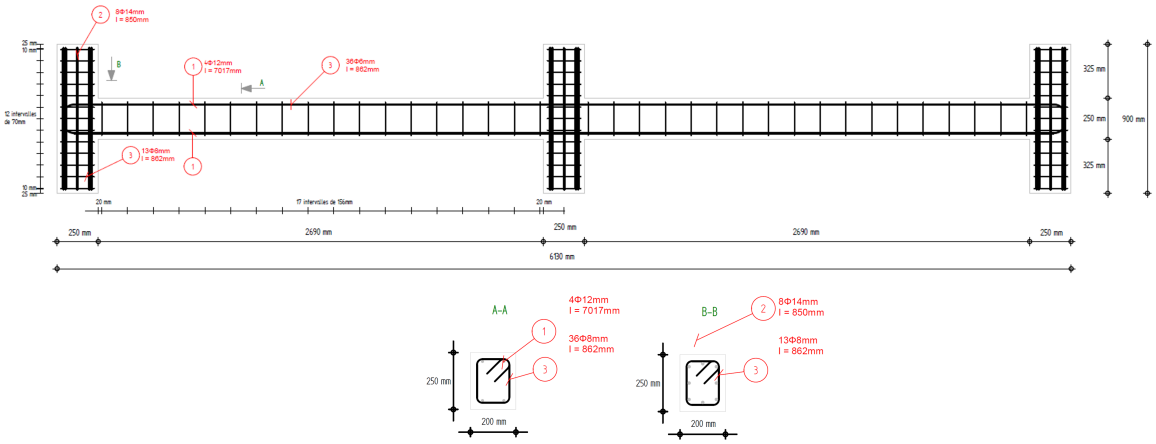

Figure 5: Beam and reinforcement dimensions - Campaign 01, 2023

2.2.2 Campaign 01 - 2023

This campaign features better controlled, more realistic boundary conditions, as well as representative RC beam size, geometry and design. Mechanical effects such as Tensile Catenary Action (TCA) and Compressive Arch Action (CAA) should be observed. The latters greatly influence a building's response during progressive collapse [1].

RC beam characteristics Beams feature specifically designed beam-column nodes. Dimensions are described in Figure (5). They are designed according to Eurocode 2 recommendations, regarding Service Limit State (SLS) and Ultimate Limit State (ULS). Variable design load is a $4.50 \cdot 10^3 N.m^{-2}$ surface load (which corresponds to a $26.4 \cdot 10^3 N.m^{-1}$ linear load). The concrete used is *C25/30-XC1-S3*, with *CEM I 52.5 N* cement. Steel rebars are *HA500 B*.

All beams will be tested after more than 28 days of curing. $16 \cdot 32cm^2$ cylindrical samples will be tested along with each beams. Steel reinforcement samples will also be tested, equipped with strain-gauges.

Experimental setup Ten structural members will be tested. Specific Boundary Conditions (BCs) have been developed, coming as close as possible to ideal embeddings. BCs will be instrumented to get transiting efforts. The hydraulic actuator will press on the central node's

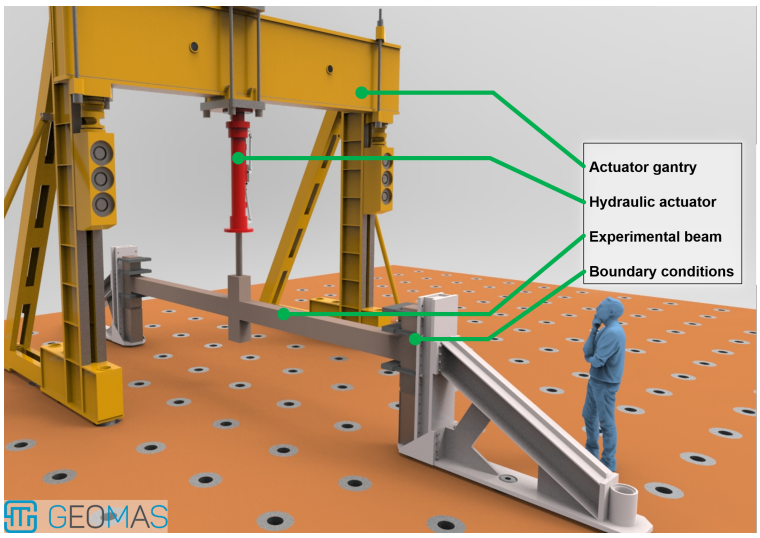

Figure 6: Experimental setup - Campaign 01, 2023

post, with force and displacement measured. 8 strain-gauges are glued on each beam's steel reinforcements. Lasers and LDVT displacement sensors, as well as speckled surfaces and camera with Digital Image Correlation (DIC) will complete the measuring apparatus. The general setup is represented in Figure(6).

3 RESULTS

3.1 Campaign 00 - 2021

3.1.1 Multi-fiber FEM comparison model

A full numerical FE model has been used to validate the proposed approach. Multi-fiber FEs were used for the numerical comparison to the experiments. The *ATL4S* platform was used[4]. *Timoshenko* kinematics [5], concrete behavior based on the works of Laborderie [6], steel behavior based on a 1D model from Menegotto and Pinto [7]), and a *Newmark* integration scheme were used. For the sub-structured PsD test comparison, the numerical part remains modeled by *Euler-Bernoulli* kinematics with a linear behavior. Details of the numerical model can be found in [8].

3.1.2 Pushovers

In total, 4 curves are obtained, as the PsD tests on `Beam4PsDB` and `Beam3PsDSS` also give force-displacement graphs. Mean stiffness and yield force are as follow: $K^I = 5.37 \cdot 10^6 N.m^{-1}$ ($\pm 20\%$) and $F_y = 57.5 \cdot 10^3 N$ ($\pm 5\%$). Figure (7) shows the force-displacements curves for all four beams. Those results were used to calibrate the numerical model described above.

3.1.3 Classic PsD

Very good agreement between numerical and experimental results can be observed in Figure (8). Although the beam suffers significant damage, the beam's behavior is well depicted by the model. Slightly larger displacements and vibration period can be explained by the lower numerical stiffness (calibrated using the pushovers results). In terms of efforts, the yield plateau is very well reproduced.

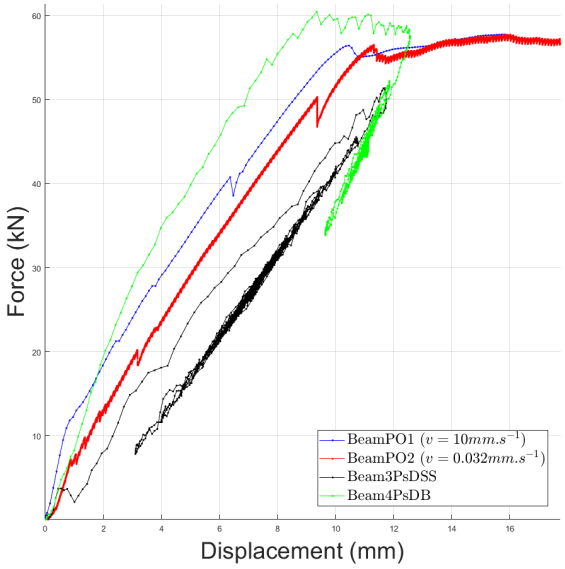

Figure 7: Force displacement curves of all beams

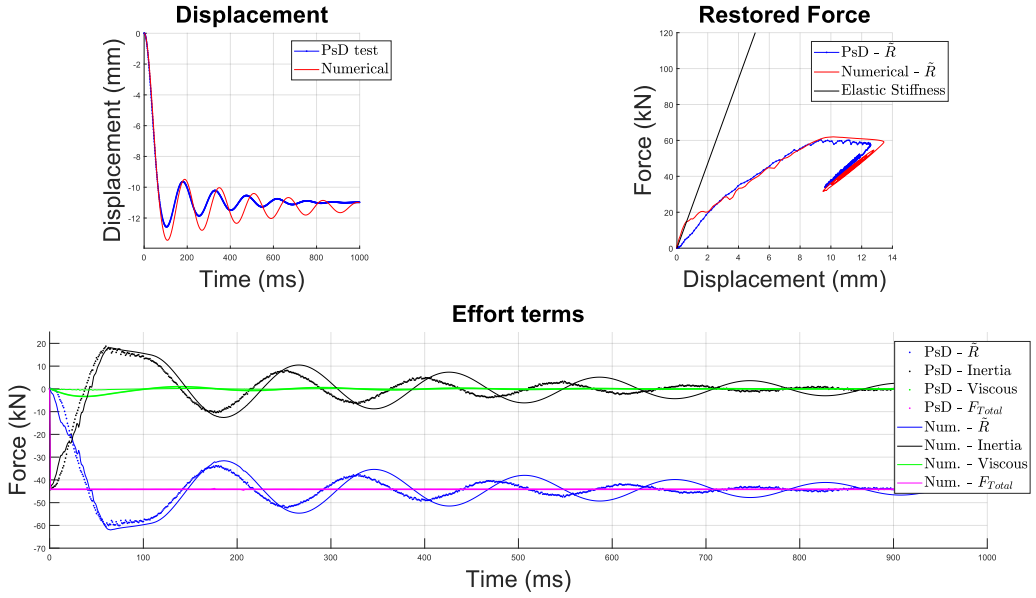

Figure 8: Experimental and numerical results, classic PsD test (`Beam4PsDB`)

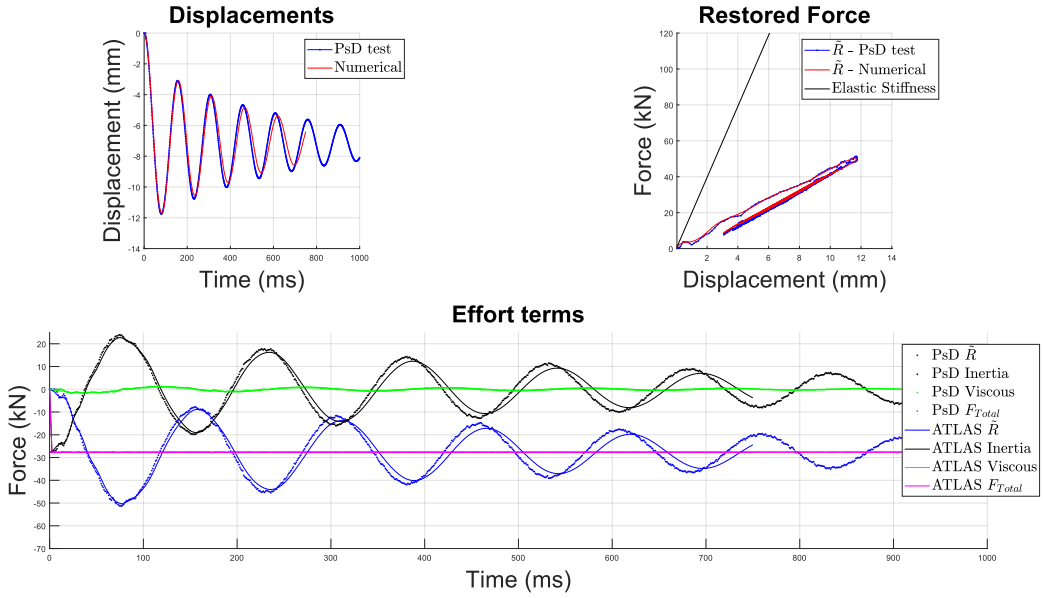

Figure 9: Experimental and numerical results, sub-structured PsD test (`Beam3PsDSS`)

3.1.4 Sub-structured PsD

Once again, the agreement between the model and the tested beam is very satisfactory, as shown in Figure (9). Displacements and vibration period are precisely represented by the numerical model. Furthermore, the internal efforts redistribution due to sub-structuring can be noted, as plastic damages on the beam are much lower than for the classic PsD test.

4 CONCLUSION AND PERSPECTIVES

4.1 Conclusion

A new way to assess the effect of loss of bearing capacity on civil engineering structures is proposed. The method is based on sub-structured Pseudo-Dynamic testing.

A very good agreement between non-linear multi-fiber models and experimental data is observed. Indeed, once calibrated, the same set of parameters is sufficient to describe the two different PsD tests (classical and sub-structured methods). In addition, pushover tests have shown that the structure's response is strain-rate independent. This legitimates the use of PsD testing, proving its robustness and showing its interest.

One of the method's main advantage is the setup's reduced cost and complexity. Physical tests are done only on the most affected parts, whilst still accounting for the remaining structure's influence. Sub-structured PsD tests on critical parts allows for a better capture of the non-linear response, compared to complex numerical models, which can prove tricky to calibrate when depicting severe non-linearities.

Another very important aspect is the methods' ability to numerically account for the and inertial forces. Thus, the dynamic response's analysis for full scale buildings is feasible using mainstream instrumentation rather than high-speed, high efforts, and high acquisition rate equipment. Tests' safety and control are improved, allowing for reproducible experiments.

4.2 Campaign 01's perspectives

As of the redaction of this paper, Campaign 01 is still underway. However, experimental results should yield answers regarding the method's ability to reproduce progressive collapse events on reinforced concrete civil engineering structures.

Larger experimentally tested sub-structured, with improved geometry and well designed beam-post integration will better represent real-life structures. Work on the boundary conditions' designs will also depict more realistically interactions between the tested sub-structure and the rest of the building. Physical phenomena such as Compressive Arch Action (CAA) and Tensile Catenary Action (TCA) should be observed. Futhermore, attention has been put on the beams' design following Eurocode 2 recommendations. The latter is driven by a realistic Service Limit State (SLS). The beams' properties come as close as possible to those of structural parts encountered in real estate.

Moreover, work on the simulated part will be done, as extension to non-linear numerical response is rather straight-forward for moderate damage representation. More extensive testing on concrete and steel samples should enable for good numerical calibration.

Finally, more instrumentation has been put in place: strain-gauges on reinforcements and boundary conditions, cameras, and a wider array of laser and LVDT displacement sensors.

REFERENCES

[1] J. Adam, F. Parisi, J. Sagaseta, and X. Lu. Research and practice on progressive collapse and robustness of building structures in the 21st century. *Engineering Structures*, 173:122–149, 2018.

[2] D. Combescure and P. Pegon. α-operator splitting time integration technique for pseudo-dynamic testing : Error propagation analysis. *Soil Dynamics and Earthquake Engineering,*, 1997.

[3] P. Pegon and A. Pinto. Pseudo-dynamic testing with substructuring at the elsa laboratory. *Earthquake Engng Struct. Dyn.*, 29:905–925, 2000.

[4] S. Grange. Atl4s plateform (a tool and language for simplified structural solution strategy). Technical report, INSA Lyon, 2009-2021.

[5] P. Kotronis and J. Mazars. Simplified modelling strategies to simulate the dynamic behaviour of rc walls. *Journal of Earthquake Engineering*, 9 (2):285 – 306, 2005.

[6] C. LaBorderie. *Phenomenes unilateriaux dans un materiau endommageable modélisation et application á l'analyse de structures en béton*. PhD thesis, Université Pierre et Marie Curie, 1991.

[7] M. Menegotto and P. Pinto. Method of analysis of cyclically loaded rc plane frames including changes in geometry and non-elastic behavior of elements under normal force and bending. Technical Report 13, Preliminary Report IABSE, 1973.

[8] D. Bertrand, S. Grange, and J.-B. Charrié. Progressive collapse analysis of rc frame building based on pseudo-dynamic (psd) testing with sub-structuring. *Journal of Building Engineering*, 52:104420, 2022.